Monthly Notices
of the
ROYAL ASTRONOMICAL SOCIETY

Mon. Not. R. Astron. Soc. **427,** 1168–1174 (2012) doi:10.1111/j.1365-2966.2012.22015.x

The first optical light from the supernova remnant G182.4+4.3 located in the Galactic anticentre region

A. Sezer,[1,2]★ F. Gök[3]★ and E. Aktekin[4]★

[1]*TÜBİTAK Space Technologies Research Institute, ODTU Campus, Ankara 06531, Turkey*
[2]*Boğaziçi University, Faculty of Art and Sciences, Department of Physics, İstanbul 34342, Turkey*
[3]*Akdeniz University, Faculty of Education, Antalya 07058, Turkey*
[4]*Akdeniz University, Faculty of Sciences, Department of Physics, Antalya 07058, Turkey*

Accepted 2012 August 29. Received 2012 August 13; in original form 2012 March 9

ABSTRACT

We report the discovery of optical filamentary and diffuse emission from G182.4+4.3 using the 1.5-m Russian–Turkish telescope. We present the optical CCD images obtained with the Hα filter, revealing the presence of mainly filamentary structure to the north-west and filamentary and diffuse structure in the centre, south and north regions of the remnant. The bright optical filaments located in the north-west and south regions are well correlated with the prominent radio shell of the remnant, strongly suggesting an association. From the flux-calibrated CCD imaging, the average [S II]/Hα ratio is found to be $\sim$0.9 and $\sim$1.1 for south and north-west regions, respectively, which clearly indicates that the emission originates from shock-heated gas. We also present the results of X-ray data obtained from *XMM–Newton*, showing diffuse emission with a very low luminosity of $\sim 7.3 \times 10^{31}$ erg s^{-1} at a distance of 3 kpc in the 0.3–10 keV energy band. Furthermore, we find a surprisingly low age of $\sim$4400 yr for this remnant, given its large radius of $\sim$22 pc.

Key words: ISM: individual objects: G182.4+4.3 – ISM: supernova remnants – X-rays: ISM.

1 INTRODUCTION

There are 274 Galactic supernova remnants (SNRs) catalogued in Green (2009) by their radio emission. Most of them are located in the Galactic plane, where the density of gas and dust is very high, which makes the observation of SNRs hard except in the radio band, due to strong interstellar extinction and reddening effects in their line of sight. This difficulty can be surmounted by using narrow-band filters such as Hα, [S II], [N II] and [O III] centred on characteristic emission lines for deep exposures. A number of Galactic SNRs have been detected with the Hα filter in particular (e.g. Mavromatakis, Xilouris & Boumis 2007; Stupar, Parker & Filipović 2007; Boumis et al. 2009; Stupar & Parker 2009; Fesen & Milisavljevic 2010), in which they usually have peculiar morphological structures. Some of them have filamentary structure while others have filamentary and diffuse structures together or arc (shell) structures. Stupar & Parker (2011) reported a catalogue of 24 known Galactic SNRs uncovered in Hα light using the Anglo-Australian Observatory/United Kingdom Schmidt Telescope (AAO/UKST) Hα survey of the southern Galactic plane. The optical observations of Galactic SNRs enable us to study the physical conditions in the remnant and the ambient medium, such as the variation of chemical composition, density and evolutionary state.

Galactic SNR G182.4+4.3, located in the anticentre region, has been detected at 1400, 2675, 4850 and 10 450 MHz with the Effelsberg 100-m telescope in the radio band by Kothes, Fürst & Reich (1998). They reported that the remnant has a shell structure with a radio spectral index of $\alpha = -0.42 \pm 0.10$ ($S_\nu \sim \nu^\alpha$), is about 50 arcmin in size, has very low radio surface brightness (7.5×10^{-23} W m^{-2} Hz^{-1} sr^{-1} at 1 GHz) and is in the Sedov expansion stage. Expansion into an ambient medium of low density indicated that its location was in front of the outer spiral arm III. H I line observations of neutral hydrogen showed that the column density towards the remnant must be $\leq 4 \times 10^{21}$ cm^{-2}. Considering its low ambient density and assuming its distance to be 3 kpc, they argued that the z-height of the remnant was about 230 pc and concluded that it was most likely the remnant of a Type Ia supernova explosion. They have searched the *ROSAT* All-Sky Survey at the position of this remnant and detected no visible X-ray emission (with a corresponding upper limit of 6.2×10^{-2} count s^{-1}). Assuming an initial explosion energy of 10^{51} erg, they obtained ambient density $n_0 \sim 0.013$ cm^{-3}, swept-up mass $M_{\rm sw} \sim 14\,{\rm M}_\odot$, electron temperature $kT \sim 5.0$ keV, age 3800 yr and shock velocity $V_{\rm exp} = 2300$ km s^{-1}.

There is no optical identification of G182.4+4.3 in the literature so far. In this paper, we report the first detection of optical emission from G182.4+4.3: both filamentary and diffuse structure in Hα.

★E-mail: aytap.sezer@boun.edu.tr (AS); gok@akdeniz.edu.tr (FG); eaktekin@akdeniz.edu.tr (EA)

© 2012 The Authors
Monthly Notices of the Royal Astronomical Society © 2012 RAS

Downloaded from https://academic.oup.com/mnras/article/427/2/1168/975414 by Akdeniz University user on 20 September 2021

Table 1. The characteristics of interference filters and exposure times of imaging observations taken with the TFOSC CCD.

Filter	Wavelength (FWHM) (Å)	Exposure times (s)
Hα	6563 (88)	900
Hα cont.	6446 (130)	900
[S II]	6728 (70)	900
[S II] cont.	6964 (300)	900

We also study *XMM–Newton* data to investigate its properties in the X-ray band and combine optical imaging and X-ray observation to present a better view of this SNR.

The paper is organized as follows. Observations and data reduction are described in Section 2. Based on the CCD imaging analysis, together with X-ray results, we discuss the filamentary and diffuse structure and the plasma parameters of the SNR in Section 3. We give our conclusions in Section 4.

2 OBSERVATIONS AND DATA REDUCTION

2.1 Optical imaging

Optical CCD imaging observations of G182.4+4.3 were taken on 2011 February 5, 2011 March 2 and 2012 February 19, with the low-resolution TUG Faint Object Spectrograph and Camera (TFOSC) equipped with a 2048 × 2048 back-illuminated camera with a pixel size of 15 × 15 μm^2 in a 13.5 × 13.5 $arcmin^2$ field of view (FOV) attached to the Cassegrain focus of the 1.5-m Russian–Turkish joint telescope (RTT150)[1] at TÜBİTAK National Observatory (TUG) Türkiye, Antalya. The optical images were obtained with Hα, [S II] and their continuum filters. The characteristics of these interference filters are summarized in Table 1. The images were reduced by using standard IMAGE REDUCTION AND ANALYSIS FACILITY (IRAF) routines for background subtraction, flat-fielding, trimming and continuum subtraction. The spectroscopic standard star HR 5501 (Hamuy et al. 1992, 1994) was used for absolute flux calibration. We write the coordinate information into the FITS header of the individual images with world coordinate system (WCS) tools. The weather conditions during these imaging observations were poor.

Due to its large size, we divided the whole remnant into several fragments and observed each fragment with the Hα filter with a short exposure time of 100 s. We obtained optical emission only from four regions, namely the north (N), north-west (NW), centre (C) and south (S). We focused our study on these four regions to obtain images with Hα, [S II] and their continuum filters with relatively long exposures (900 s). Continuum-subtracted Hα images of NW, S, C and N regions are given in Figs 1, 2 and 3.

We also took long-slit spectra by locating the slit on the brightest filament in the S region on 2011 November 7 with an exposure time of 7200 s, with the spectroscopic mode of the TFOSC attached to the Cassegrain focus of the RTT150. Unfortunately, due to poor observing conditions the spectra obtained did not allow us to achieve reliable results.

[1] Details of the telescope and the spectrograph can be found at http://www.tug.tubitak.gov.tr.

2.2 X-ray and radio-continuum observations

XMM–Newton (Jansen et al. 2001) observed G182.4+4.3 on 2001 June 15, under the observation ID 50406540 and using an exposure time of 23 ks. *XMM–Newton* has three X-ray telescopes (Aschenbach 2002), one equipped with EPIC-PN (Strüder et al. 2001) and two with EPIC-MOS (Turner et al. 2001) CCD detectors in the focal plane. The data were reduced and analysed using the XMM-NEWTON SAS,[2] version 1.52.8. Calibrated event files for the EPIC-MOS1, EPIC-MOS2 and EPIC-PN detectors were produced using SAS tasks EMCHAIN and EPCHAIN and following standard procedures. An EPIC-MOS2 image in the 0.3–10 keV energy band of G182.4+4.3 is given in Fig. 4.

The overall radio structure of G182.4+4.3 at 4850 MHz with the Effelsberg 100-m telescope (R. Kothes, private communication) is given in Fig. 5. As seen from the figure, the radio shell is most prominent in the south-west direction; this is because the prominent part of the shell is expanding towards the Galactic plane into a higher density medium while the top shell is expanding away from the plane into a very low-density medium (Kothes & Brown 2009).

We overlaid the Hα mosaic image of the observed regions with a radio-continuum contour image taken from 4850-MHz Effelsberg data and an X-ray contour image from *XMM–Newton* data to see if there is an association between the optical, radio and X-ray emission. As seen from Fig. 6, there is a good correlation between optical and radio emission in the NW and S regions. Due to poor observing conditions, for the N and C regions the correlation is not seen clearly. The optical emission of the S region correlates with both the radio and X-ray emission. N, NW and C regions are situated out of the FOV of *XMM–Newton*.

3 RESULTS AND DISCUSSION

We present the first CCD images of G182.4+4.3, together with the results from *XMM–Newton* archival data analysis.

The Hα image of the NW region shows mainly filamentary structure while that of other regions shows both filamentary and diffuse structure; see Figs 1, 2 and 3. As seen from Fig. 1, strong multiple filaments overlapping with the surrounding diffuse emission are visible only in the lower left part of the NW region. In the S region (see Fig. 2), a strong and long filamentary structure extending from the south-east edge of the field up to the north-west edge is visible. There is also a weaker filament extending parallel to the previous one in the south-west edge of this region. In the upper part of the prominent filament, strong diffuse emission is visible. In the C region (see Fig. 3, upper panel), there is a curved weak filament extending from south to north-west as well as fainter diffuse emission. The reason for the weakness of the emission may be the presence of very bright stars in this field. The N region (see Fig. 3, bottom panel) seems much more complex in Hα emission compared with other regions. There are several small-scale filaments embedded in the diffuse emission in this region. The filaments seen in the NW and S regions are very well correlated with the prominent radio shell of the remnant.

An [S II]/Hα ratio greater than 0.5 is used as a standard discriminator for shock-heated gas and hence is indicative of SNRs (Fesen, Blair & Kirshner 1985). We obtained [S II]/Hα ratios of 0.9 ± 0.1 and 1.1 ± 0.1 for S and NW regions, respectively. These ratios indicate that the emission originates from the ionization of shock-heated gas resulting from collision.

[2] Science Analysis Software (SAS), see http://xmm.vilspa.esa.es/sas/.

Downloaded from https://academic.oup.com/mnras/article/427/2/1168/975414 by Akdeniz University user on 20 September 2021

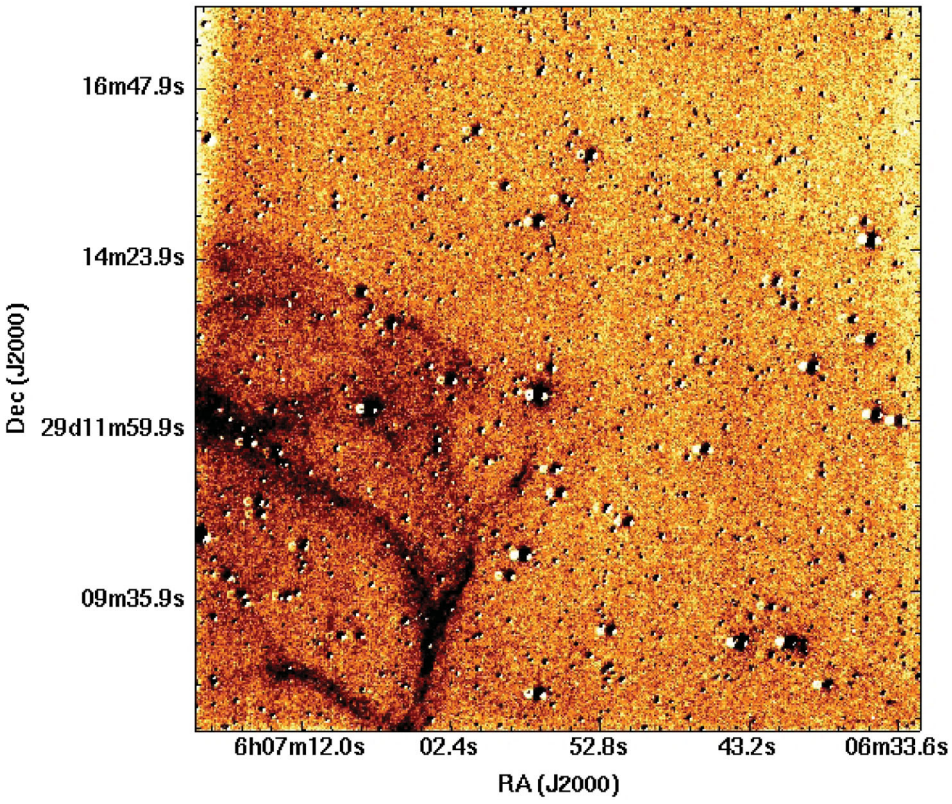


Figure 1. Continuum-subtracted and smoothed Hα image of the NW region. A network structure of filaments is seen in the lower left part of this image.

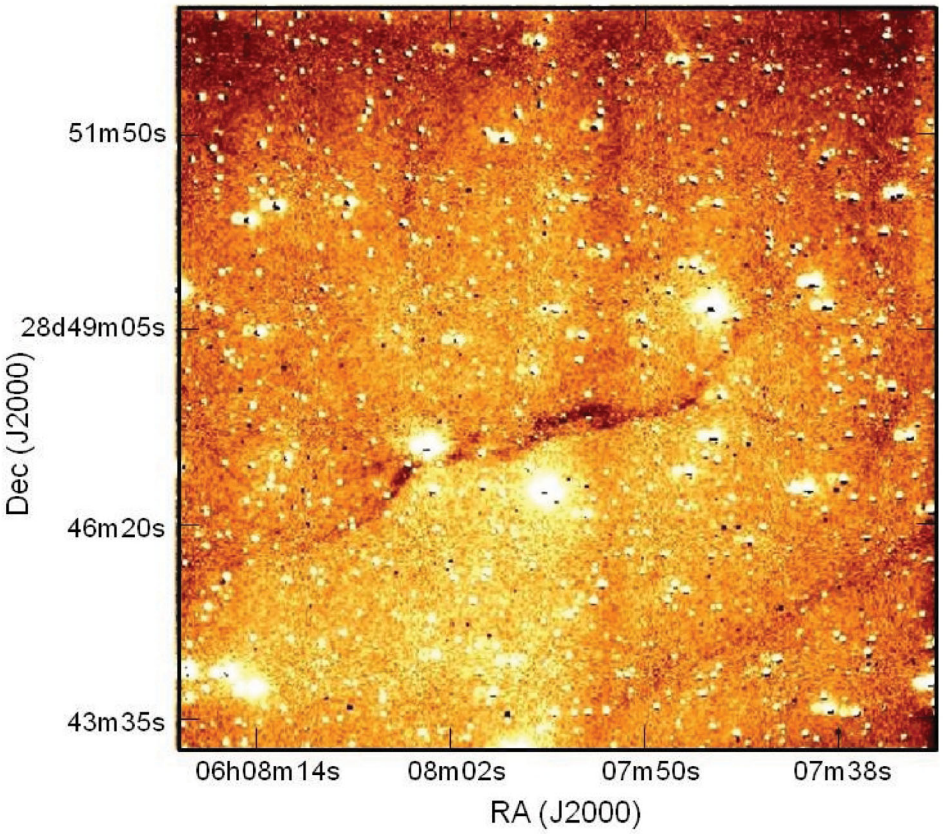


Figure 2. Continuum-subtracted and smoothed Hα image of the S region. A long and sharp filament, which is $\sim$8 arcmin in extent, is noticeable in this figure.

Downloaded from https://academic.oup.com/mnras/article/427/2/1168/975414 by Akdeniz University user on 20 September 2021

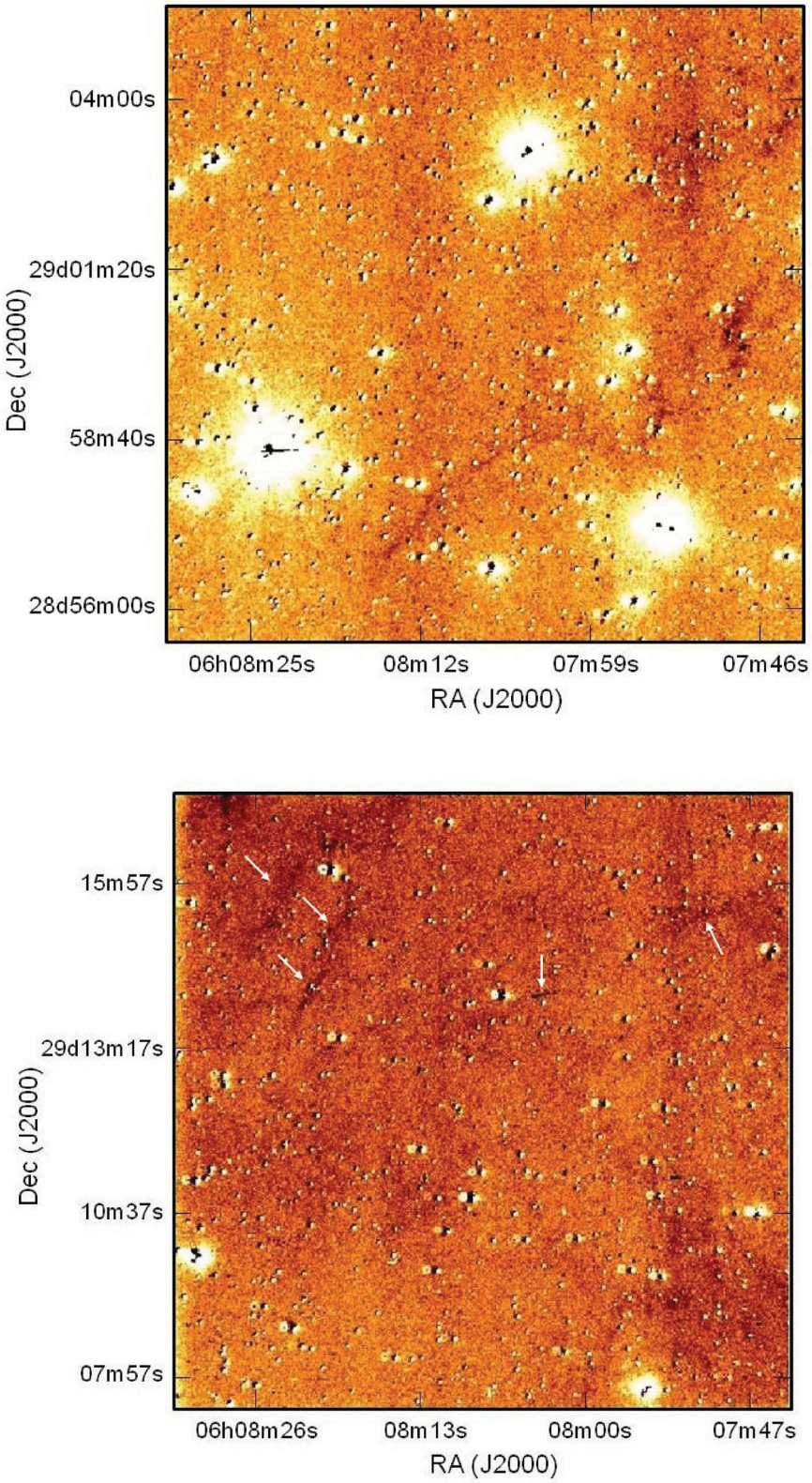


Figure 3. The upper and lower panels show continuum-subtracted and smoothed Hα images of the C and N regions, respectively. Filamentary structure is noticeable in the C region, while both filamentary (indicated with arrows) and diffuse structure are present in the N region.

We detected diffuse and faint X-ray emission coming from the remnant, as seen from Fig. 4, and obtained a background-subtracted count rate of 0.04 count s^{-1}. Even with this low-count X-ray detection, we tried to obtain some information on the X-ray nature of G182.4+4.3 using the EPIC-MOS1 spectrum. We extracted the spectrum from a circular region with a radius of 8.3 arcmin centred at RA(2000) = $06^{h}07^{m}10^{s}$, Dec. (2000) = $28^{\circ}52'05''$. The spectrum was grouped with a minimum of 30 count bin^{-1} and we used

© 2012 The Authors, MNRAS **427,** 1168–1174
Monthly Notices of the Royal Astronomical Society © 2012 RAS

Downloaded from https://academic.oup.com/mnras/article/427/2/1168/975414 by Akdeniz University user on 20 September 2021

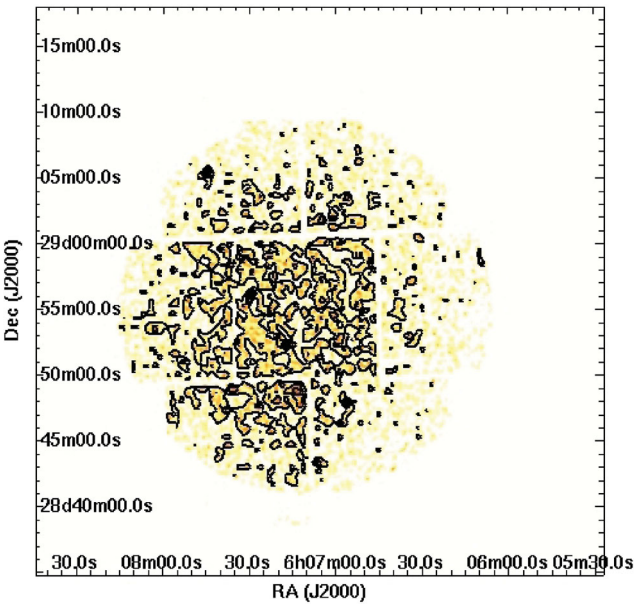


Figure 4. The EPIC-MOS2 image of G182.4+4.3 in the 0.3–10 keV energy band with X-ray contour levels of 2, 2.86, 4.09, 5.85 and 7 counts pixel^{-1}.

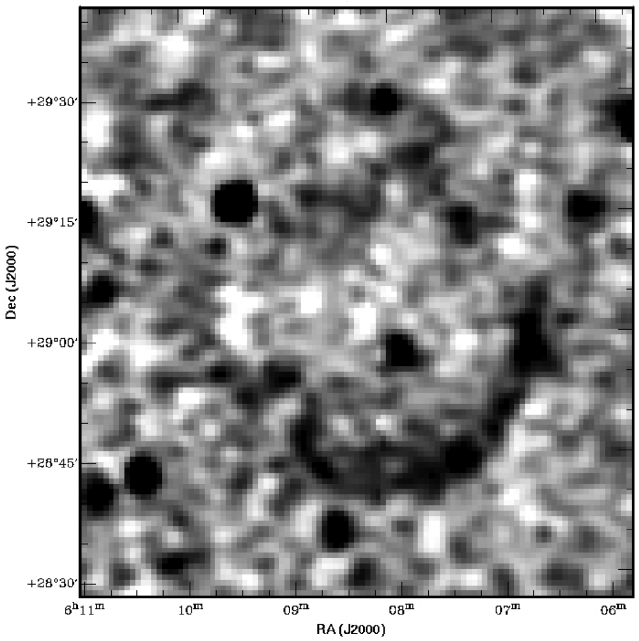


Figure 5. The radio-continuum image taken from 4850-MHz Effelsberg data. A typical shell with a diameter of about 50 arcmin.

χ^2 statistics. The spectrum was best fitted with the VPSHOCK model, which is suitable for modelling plane-parallel shocks in young SNRs where the plasma has not reached ionization equilibrium (Borkowski, Lyerly & Reynolds 2001), modified by Galactic absorption via the WABS multiplicative model (Morrison & McCammon 1983) using XSPEC v11.3 (Arnaud 1996). During model fitting, the absorbing column density ($N_{\rm H}$), electron temperature ($kT_{\rm e}$) and ionization parameter ($\tau = n_{\rm e}t$) were set free while all elements were fixed at their solar abundances (Anders & Grevesse 1989). This fitting gave us $N_{\rm H} \sim 5 \times 10^{21}$ cm^{-2}, $kT_{\rm e} \sim 0.9$ keV, $\tau \sim 0.3 \times 10^{10}$ cm^{-3} s and a low X-ray luminosity ($L_{\rm X}$) in the 0.3–10 keV energy band of $\sim 7.3 \times 10^{31}$ erg s^{-1} at a distance of 3 kpc, with an acceptable reduced χ^2 value of 1.11 (64.5/58 d.o.f.). Using the emission measure ($EM = n_{\rm e}n_{\rm H}V$, where $n_{\rm e}$ and $n_{\rm H}$ are the number densities of electrons and protons respectively and V is the X-ray-emitting volume, and assuming $n_{\rm e} = 1.2n_{\rm H}$), we obtain a significantly low electron density $n_{\rm e}$ of ~ 0.024 cm^{-3}. The mass of the X-ray-emitting gas is calculated to be $\sim 1\,{\rm M}_{\odot}$ from $M_{\rm X} = m_{\rm H}n_{\rm e}V$, where $m_{\rm H}$ is the mass of a hydrogen atom. From $t = \tau/n_{\rm e}$, the age of G182.4+4.3 is calculated to be $\sim$4400 yr, which is consistent with the age found by Kothes et al. (1998) from *ROSAT* data.

From the size distribution of the SNRs in the Magellanic Clouds, Badenes, Maoz & Draine (2010) showed that the distributions are close to uniform between $r \sim 10$ pc and $r \sim 30$ pc. They argued that a uniform size distribution arises from the physics of SNR evolution, the Sedov expansion model for SNRs and the distributions of densities in the ambient medium. Thus, since it is at age $t \sim 4400$ yr and has $r \sim 22$ pc, G182.4+4.3 is likely to be in the Sedov phase. A 4400-yr-old SNR with a given original supernova mass can expand to such a large size in a low-density medium. The location of G182.4+4.3 is high with respect to the Galactic plane ($\sim$230 pc), it has a very low radio surface brightness and is faint in X-rays, indicating that the remnant is expanding in a low-density medium. The low electron density obtained from X-ray spectral analysis, which is consistent with that of *ROSAT* data, also supports this idea. Regarding its large radius and low age, G182.4+4.3 resembles the shell-type Galactic SNRs G93.3+6.9 (DA530) and G156.2+5.7. G93.3+6.9 is located at 420 pc above the Galactic plane at a distance of 3.8 kpc and has a diameter of $D = 26$ pc (Landecker et al. 1999). It has an age of 5000 yr and is expanding in a very low-density medium (0.05 cm^{-3}). It has very low radio surface brightness and its X-ray emission is extremely faint (Landecker et al. 1999). The other example, G156.2+5.7, is located at $z > 130$ pc, at a distance of $\sim$3 kpc and is expanding in a low-density medium (0.01 cm^{-3}) (Pfeffermann, Aschenbach & Predehl 1991). Its optical observations suggest that it is interacting with a clumpy interstellar medium (Gerardy & Fesen 2007). It has low radio surface brightness; however, it is bright in X-rays. Kothes et al. (1998) compared G182.4+4.3 with the G156.2+5.7 in this respect. They argued that the difference in the X-ray luminosities of G182.4+4.3 and G156.2+5.7 may result from the difference in the ratio between the mass of the clouds and the mass of the intercloud medium. They concluded that G182.4+4.3 expanded into a medium with low density and a low fraction of clouds. Propagation of an SNR shock wave into a cool dense interstellar medium leads to Hα emission. The filamentary Hα emission emanating from this remnant suggests that there might be clumps of clouds in the medium in which the SNR is expanding. Furthermore, the different scale and structures of the filaments, together with the diffuse emission, may indicate the presence of small- or large-scale inhomogeneities in the interstellar clouds. However, in the FOV of *XMM–Newton* (see Fig 4), the cloud density might be very low, leading to faint X-ray emission.

From the optical spectra of SNRs, the electron density can be estimated by using the flux ratio of [S II](λ6716/λ6731) (Osterbrock & Ferland 2006). The estimated electron density allows us to obtain the pre-shock cloud density (see Fesen & Kirshner 1980). Future spectral observations of this remnant could give detailed information about the inhomogeneities in the SNR and its ambient medium.

4 CONCLUSION

We detected optical filamentary and diffuse emission for the first time for G182.4+4.3, with several short- or long-scale filaments

Downloaded from https://academic.oup.com/mnras/article/427/2/1168/975414 by Akdeniz University user on 20 September 2021

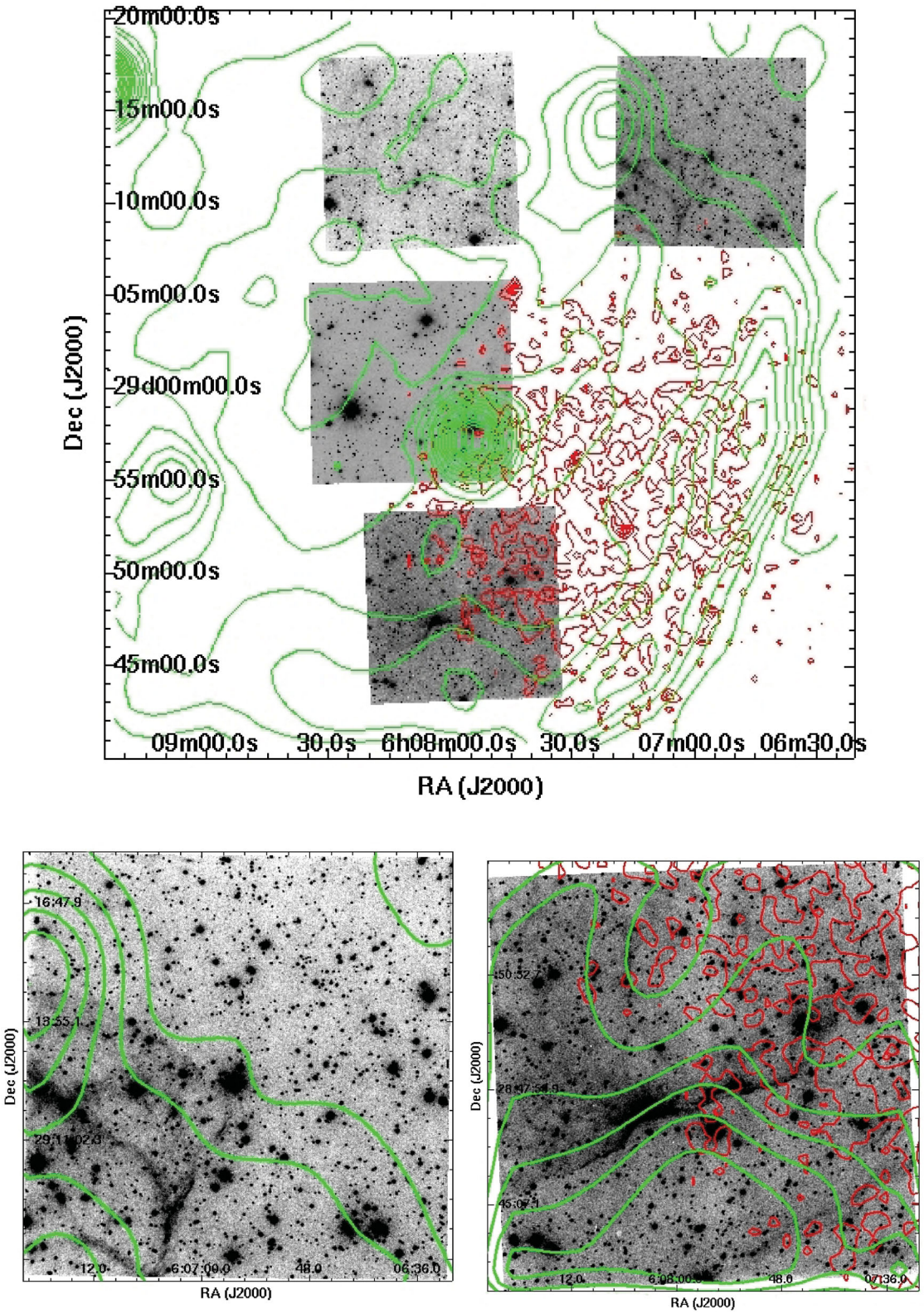


Figure 6. Upper panel: the mosaic image combines optical images (Hα) of four fields (N, NW, C and S) of G182.4+4.3 overlaid with (i) radio-continuum contours (green in the online article) taken from the 4850-MHz Effelsberg data and (ii) X-ray contours (red in the online article) from EPIC-MOS2. The radio contour levels are -2.95, 1.32, 5.59, 7.73 and 14.13 mJy beam^{-1} and the X-ray contour levels are 2.02, 2.86, 4.09, 5.85 and 7 counts pixel^{-1}. Each optical image (N, NW, C and S) covers an area of $\sim 10 \times 10$ arcmin^2. The whole figure covers an area of 40×40 arcmin^2. Lower left panel: enlarged Hα image of the NW region overlaid with radio-continuum contours (green in the online article). The contour levels are -0.67, 2.94, 6.54 and 10.14 mJy beam^{-1}. Lower right panel: enlarged Hα image of the S region overlaid with radio-continuum (green in the online article) and X-ray contours (red in the online article). The radio contour levels are 0.11, 2.09, 4.09 and 7.08 mJy beam^{-1} and the X-ray contour levels are 2.02, 2.88, 4.11 and 7 counts pixel^{-1}.

© 2012 The Authors, MNRAS **427,** 1168–1174
Monthly Notices of the Royal Astronomical Society © 2012 RAS

Downloaded from https://academic.oup.com/mnras/article/427/2/1168/975414 by Akdeniz University user on 20 September 2021

found in the N, NW, C and S regions. The strong optical filaments located in the NW and S regions match with the prominent radio shell in the 4850-MHz Effelsberg data of the remnant, suggesting their association. Very strong emission of [S II] relative to Hα ([S II]/Hα $\sim$ 0.9, $\sim$1.1) obtained from imaging suggests that the emission originates from shock-heated gas. Finally, we estimated the X-ray properties of this remnant using *XMM–Newton* archival data. The X-ray spectrum of G182.4+4.3 shows that the plasma is of thermal origin in a non-equilibrium ionization state and requires a temperature of $\sim$0.9 keV. The best fit to the spectrum implies that the SNR is very young ($\sim$4400 yr), is expanding in a very low-density medium ($\sim$0.024 cm^{-3}), has a low X-ray-emitting mass ($\sim$1 M$_{\odot}$) and a very low X-ray luminosity ($\sim$7.3 $\times$ 10^{31} erg s^{-1} in the 0.3–10 keV band).

ACKNOWLEDGMENTS

We are grateful to M. Filipovic for his constructive comments and suggestions on the manuscript. We thank TÜBİTAK for partial support in using RTT150 (the Russian–Turkish 1.5-m telescope in Antalya) with project number 09ARTT150-458-0. We also thank A. Akyüz for providing us with some of the interference filters and R. Kothes for providing us with the 4850-MHz Effelsberg data. The authors acknowledge support by the Akdeniz University Scientific Research Project Management. AS is supported by a TÜBİTAK PostDoctoral Fellowship.

REFERENCES

Anders E., Grevesse N., 1989, Geochimica Cosmochimica Acta, 53, 197
Arnaud K. A., 1996, in Jacoby G. H., Barnes J., eds, ASP Conf. Ser. Vol. 101, Astronomical Data Analysis Software and Systems V. Astron. Soc. Pac., San Francisco, p. 17
Aschenbach B., 2002, in Gorenstein P., Hoover R. B., eds, Proc. SPIE Vol. 4496, X-Ray Optics for Astronomy: Telescopes, Multilayers, Spectrometers, and Missions. SPIE, Bellingham, p. 8
Badenes C., Maoz D., Draine B. T., 2010, MNRAS, 407, 1301
Borkowski K. J., Lyerly W. J., Reynolds S. P., 2001, ApJ, 548, 820
Boumis P., Xilouris E. M., Alikakos J., Christopoulou P. E., Mavromatakis F., Katsiyannis A. C., Goudis C. D., 2009, A&A, 499, 789
Fesen R. A., Kirshner R. P., 1980, ApJ, 242, 1023
Fesen R. A., Milisavljevic D., 2010, AJ, 140, 1163
Fesen R. A., Blair W. P., Kirshner R. P., 1985, ApJ, 292, 29
Gerardy C. L., Fesen R. A., 2007, MNRAS, 376, 929
Green D. A., 2009, Bull. Astron. Soc. India, 37, 45
Hamuy M., Walker A. R., Suntzeff N. B., Gigoux P., Heathcote R., Phillips M. M., 1992, PASP, 104, 533
Hamuy M., Suntzeff N. B., Heathcote R., Walker A. R., Phillips M. M., 1994, PASP, 106, 566
Jansen F. et al., 2001, A&A, 365, L1
Kothes R., Brown J., 2009, in Strassmeier K. G., Kosovichev A. G., Beckman J. E., eds, Proc. IAU Symp. 259, Cosmic Magnetic Fields: From Planets, to Stars and Galaxies. Cambridge Univ. Press, Cambridge, p. 75
Kothes R., Fürst E., Reich W., 1998, A&A, 331, 661
Landecker T. L., Routledge D., Reynolds S. P., Smegal R. J., Borkowski K. J., Seward F. D., 1999, ApJ, 527, 866
Mavromatakis F., Xilouris E. M., Boumis P., 2007, A&A, 461, 991
Morrison R., McCammon D., 1983, ApJ, 270, 119
Osterbrock D. E., Ferland G. J., 2006, Astrophysics of the Gaseous Nebulae and Active Galactic Nuclei. University Science Books, Sausalito, CA, p. 123
Pfeffermann E., Aschenbach B., Predehl P., 1991, A&A, 246, L28
Strüder L. et al., 2001, A&A, 365, L18
Stupar M., Parker Q. A., 2009, MNRAS, 394, 1791
Stupar M., Parker Q. A., 2011, MNRAS, 414, 2282
Stupar M., Parker Q. A., Filipović M. D., 2007, MNRAS, 374, 1441
Turner M. J. L. et al., 2001, A&A, 365, L27

This paper has been typeset from a TEX/LATEX file prepared by the author.

Downloaded from https://academic.oup.com/mnras/article/427/2/1168/975414 by Akdeniz University user on 20 September 2021